Khurgin, J.B.; Petrov, A.; Eich, M.; Uskov, A.V.:

**Direct Plasmonic Excitation of the Hybridized Surface States in Metal Nanoparticles.**

In: ACS Photonics. Vol. 8 (2021) 7, 2041 - 2049.

First published online by ACS: 12.06.2021

https://dx.doi.org/10.1021/acsphotonics.1c00167

# Direct Plasmonic Excitation of the Hybridized Surface States in Metal Nanoparticles

Jacob B Khurgin,* Alexander Petrov, Manfred Eich, and Alexander V. Uskov

**ABSTRACT:** Plasmon driven chemical reactions are a subject that is currently capturing the attention of the research community and generates a fair amount of arguments about their origin. Taking into account that the lifetime of excited hot carriers in metals is very short, some mechanism is required to store carriers long enough and in sites that allow chemical reactions with the environment. One established mechanism is the injection of charges into either the valence or conduction band of a semiconductor, followed by a chemical reaction at the semiconductor surface. Here, we consider a somewhat less explored pathway by which plasmon decay can cause a chemical reaction: the direct excitation of hybridized surface states by plasmons. Using a simple model, we evaluate theoretically the rate of direct excitation and find that it can be comparable and often exceed the rate of indirect excitation of surface states. Our findings correspond to prior experimental results. We also identify the conditions under which one can enhance the direct excitation efficiency and, thus, bring plasmon driven photochemistry closer to practical applications.

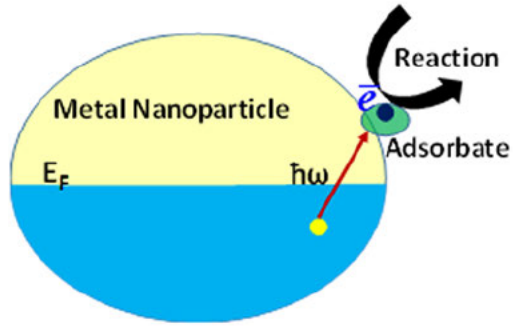


Since the turn of the millennium, the interdisciplinary field of plasmonics has been attracting the growing interest of scientists and engineers from different walks of life, mostly because plasmonics potentially enables the concentration of optical fields into volumes well below the diffraction limit, thus, opening a plethora of potential applications in nanoscale interconnects, sources, detectors, sensors, and other integrated optoelectronic devices.[1,2] In recent years, though, the enthusiasm has somewhat cooled off, as it was recognized that the subwavelength concentration of optical energy in the metal nanostructures is inevitably accompanied by the massive loss that limits the plasmon (or, more precisely, surface plasmon polariton − SPP) lifetime to tens of femtoseconds.[3] With losses on that scale, plasmonic devices can only be competitive in very specific applications, where energy efficiency is not the defining factor, such as sensing,[4,5] quantum emitters,[6] and a few others. Fortunately, as the inconvenient truth of the inherently large loss in metals had settled in, it was realized by many in the community that, rather than being an impediment, this loss can be harnessed to perform useful functions,[7] such as infrared detection,[8] photothermal therapy,[9] and, most appealing, photocataly sis.[10−12]

Significant advances have been made in the plasmon derived catalysis, however, the subject remains controversial, and so far, there has emerged no universally accepted physical picture of what processes actually lead to the observed acceleration of chemical reactions.[13] Perhaps, the least controversial is the situation when the carriers excited by plasmon decay get injected into the established catalytic material, typically a semiconductor or dielectric such as $TiO_2$ and all the subsequent chemical activity takes place on the surface of that catalyst.[14] In $TiO_2$ direct UV excitation revealed life times of carriers at the crystal surface exceeding several hundred nanoseconds and that photocatalytic activity linearly scales with these lifetimes.[15] The fact that plasmon excited carriers can surpass potential barriers and get injected into the adjacent semiconductor[16] is well established and confirmed by measuring substantial photocurrent in numerous plasmonic detectors.[8,17] In other cases, quite often chemical reaction takes place on the surface of the metal itself,[11] or on the molecules (adsorbates) attached to the metal surface as shown in Figure 1a. That requires the excited carriers to have large energy (nearly) resonant with the discrete energy level of the surface complex, and, crucially, it requires the injection to take place before the energy of the carriers is depleted by the carrier−carrier scattering that occurs on the scale of tens of femtoseconds.[18] Once a few carrier−carrier interactions take place the quasi equilibrium that lasts for a few picoseconds (time of energy transfer from carriers to the lattice) is

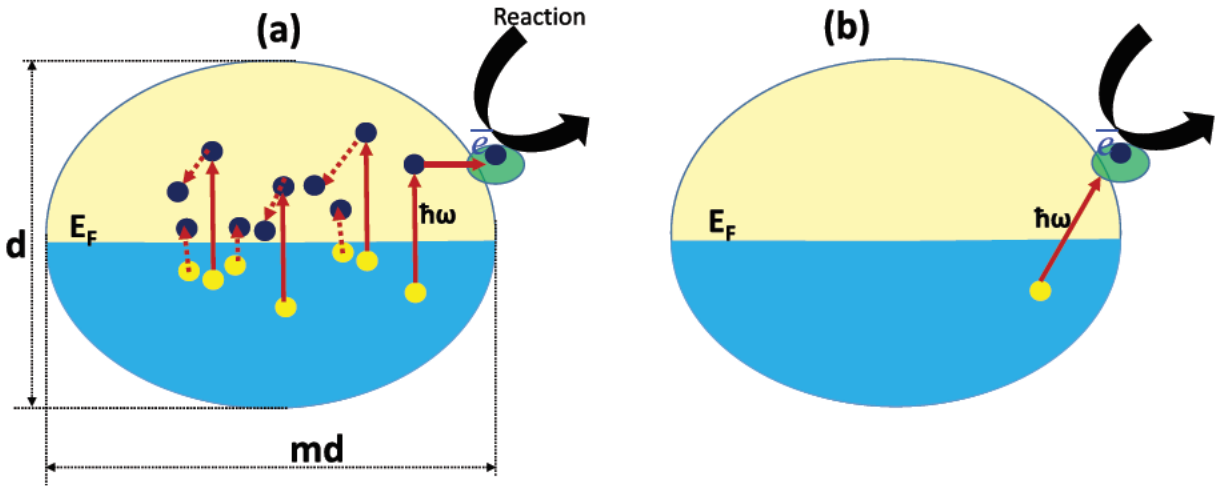


**Figure 1.** (a) Indirect excitation: Chemical reaction initiated by a plasmon excited ballistic carrier tunneling into the hybrid adsorbate state on the surface. Dashed lines indicate energy relaxation via carrier−carrier scattering (b) Direct excitation: Chemical reaction initiated by direct transfer of carriers onto the surface states. The process leads to additional plasmon damping, so called chemical interface damping (CID).

established and can be (approximately) characterized by the electron temperature $T_e$. But the energy of the thermalized electrons under practical (i.e., not high power laser pulse) illumination is low, and calling them "hot" is a misnomer, as they are "lukewarm" at best,[19] as demonstrated in recent experimental measurements.[20] It is easy to see that each collision of "hot" and "cold" carriers generates three new carriers (as shown by dashed lines in Figure 1a), so the energy of the initial hot carrier is split three ways which typically makes it too low for one of the carriers to be injected into surface complex and cause a chemical reaction. That is why in a number of recent publications[21−24] the entire concept of "hot carrier induced photocatalysis" has been put in doubt, and all the numerous observations of plasmon enhanced chemical reactions have been attributed to the conventional thermal effects, that is, associated with the lattice and not due to the generation of hot electrons. This declaration, while possibly correct for some specific experimental results, is generally erroneous, as it confuses the "not so hot" carriers thermalized at $T_e$ and incapable of any catalytic action with the "ballistic" carriers that have not yet experienced carrier−carrier collisions, and, having energies of up to $\hbar\omega$, are perfectly capable of reaching the surface states where chemical reactions take place. This difference has been discussed at length in[19,25]

The aforementioned ballistic carriers are excited when the SPP decays via different mechanisms, such as interband absorption, phonon assisted absorption, electron−electron scattering assisted absorption via Umklapp process, and Landau damping (LD), also known as surface scattering assisted absorption.[18,26,27] Of all these processes, it is the last one that contributes most to the injection and chemical reactions taking place at the surface, because the carriers are excited directly near the surface rather than in bulk where, on their way toward the surface, they would likely encounter an electron−electron scattering event. In case of small nano particles with dimensions comparable or less than mean free path of electron−phonon collision (about 10−20 nm) and of the mean free path of electron−electron scattering which, for a few eV of electron energy is of the same magnitude, LD is the dominant decay mechanism, but since only a small fraction of carriers gets excited at a right place (where the chemically active adsorbate resides) and with a right energy, the efficiencies of plasmon driven reactions remain abysmally low. The situation is explained in Figure 1a where one can see how only a very few of the excited carriers get transferred to the surface states while most of them will decay as shown by dashed lines.

But, as the adsorbate state, molecular moiety, is hybridized with the metal states and thus has nonzero overlap with them, as shown in Figure 1b, there exists an alternative mechanism by which the electrons can be directly transferred from below Fermi level into the hybridized surface state.[28−30] Since this additional energy loss channel accelerates plasmon decay it also broadens the line width of the plasmon resonance and, hence, is often referred to as chemical interface damping (CID)[31] as well as "Coherent electron transfer".[32] It should be mentioned that CID might be a result of two effects. First, there might be an electron transfer into the adsorbate,[33,34] and second, there might be additional plasmon decay due to electron scattering caused by an adsorbate induced effective roughness of the surface. Differentiation between these two mechanisms can be done by spectral investigation of damping, as electron transfer mechanism jumps in only at certain minimal photon energy and surface roughness mechanism is broadband and is present even at DC excitations where it shows up as resistivity increase.[35−37] But due to the concentration on nanoparticles, the CID was investigated up to now only at frequencies of SPP resonance, and a differentiation between the two effects is difficult. Recently it was shown that CID due to thiol adsorbates might be connected to the dipole moment of the adsorbed thiol molecules.[38] Based on a theoretical estimation, a charge transfer mechanism was excluded as the reason for CID in this case.[38] Here we present a new theoretical approximation for the mechanism connected to charge transfer. There is also a prior estimation by Persson.[39] We go beyond this study by evaluating the strength of transition by applying the Fermi golden rule and estimating quantum mechanical matrix elements for the indirect in real space transition.

Possibility of direct excitation of adsorbates has been raised in a number of works, and the experimental evidence has been accumulating.[33,38,40−45] Recently, for example, it was shown

that the photocurrent from nanoporous gold depends on the existence of −OH adsorbates at the surface.[30] But no theoretical estimate, no matter how rough, has been made of the efficiency of this direct process in comparison to the sequential process shown in Figure 1a. In this work we provide such an estimate by introducing a very simple, yet not unreasonable model based on Fermi Golden rule, test it against available experimental data, and conclude that direct process can be at least as efficient as sequential one, especially for the elongated nanoparticles. We show that the CID due to charge transfer can also explain additional plasmon damping observed in experimental works.[38,41,46] In addition, we show in the Supporting Information (SI) that the other component of CID due to transition into the free carrier states assisted by the effective roughness of the surface state is significantly weaker than the direct absorption process.

## MODEL

The model is illustrated in Figure 2, and for the purpose of simplicity, following ref 47, we start with just a single metal surface and then generalize our results for more complex shapes. The molecular orbital $|mo\rangle$ of the adsorbate with energy $E_{mo}$ is assumed to have an ellipsoid like shape with the long half axis $a$ and short half axis $b$ described by a wave function

$$\Psi_{mo} = \Phi(x)\Psi_{yz}(y, z) \tag{1}$$

where the in plane wave function is taken to be Gaussian

$$\Psi_{yz} = \frac{2^{1/2}}{\pi^{1/2}a}\exp\left[-\frac{z^2 + y^2}{a^2}\right] \tag{2}$$

and the normal to interface wave function is

$$\Phi_x(x > 0) = \sqrt{\frac{2C_p}{b}}e^{-x/b} \tag{3}$$

where

$$C_p = \int_0^\infty \Phi^2(x)\mathrm{d}x \Big/ \int_{-\infty}^\infty \Phi^2(x)\mathrm{d}x \tag{4}$$

is the fraction of the electron charge of the molecular orbital overlapping with the states in the metal. If the wave function is continuous exponential both inside and outside the metal $\Phi_x(x) \sim \exp(-|x - x_0|/b)$, $C_p = 1/2\exp(-2x_0/b)$. It should be noted that these wave functions were chosen to obtain analytic expressions, but as we have verified experimentally, the end order of magnitude result does not depend much on the exact shapes of wave function as long as the values of $a$, $b$, and $C_p$ remain the same. For example, replacing Gaussian function (eq 2) with the Hermit Gaussian function or replacing the exponential function (eq 3) with a Gaussian one does not affect the end result by more than 15−20%, as shown in SI, Figure S3.

The free electron state in the metal $|k\rangle$ has the wave function

$$\varphi_k = \frac{\sqrt{2}}{L^{3/2}}\sin(k_x x)\exp[i(k_y y + k_z z)] \tag{5}$$

where $L^3$ is the quantization volume. The boundary condition taken here $\varphi_k(x = 0) = 0$ does not include the effect of spillover of electrons outside a nominal metal boundary by the distance of about $1/k_F$, that is, on the order of 1 Å, but this effect can be incorporated into the overlap factor, $C_p$.

Due to wave function overlap, $|mo\rangle$ is coupled to the continuum of states $|k_{res}\rangle$ nearly resonant with it. The interference between the light absorbed into the continuum and into the $|mo\rangle$ results in Fano resonances similar to the ones observed in all "autoionizing" discrete sates coupled to continuum.[48,49] But since in our case absorption occurs not from a discrete layer but from a continuum, all the spectral features of Fano resonance will not be observed. Furthermore, the transition between a below Fermi level state $|k\rangle$ to a state $|k_{res}\rangle$ coupled to $|mo\rangle$ is forbidden in bulk and only allowed due to discontinuity of normal electric field and wavefunction at the surface, that is, it constitutes LD, which is followed by instant (i.e. coherent) injection into $|mo\rangle$. This process has already been treated in the established model,[18] and now we concentrate our attention on less explored direct transition into $|mo\rangle$.

The matrix element of interaction Hamiltonian for the transition from the state below Fermi level $|k\rangle$ to the surface sate $|mo\rangle$ caused by optical field $E(r)\cos(\omega t)$ is

$$H_{int} = \frac{e}{2m_0}\langle k|A\cdot p|mo\rangle = \frac{\hbar e}{2m_0\omega}\langle k|\nabla|mo\rangle\cdot E \tag{6}$$

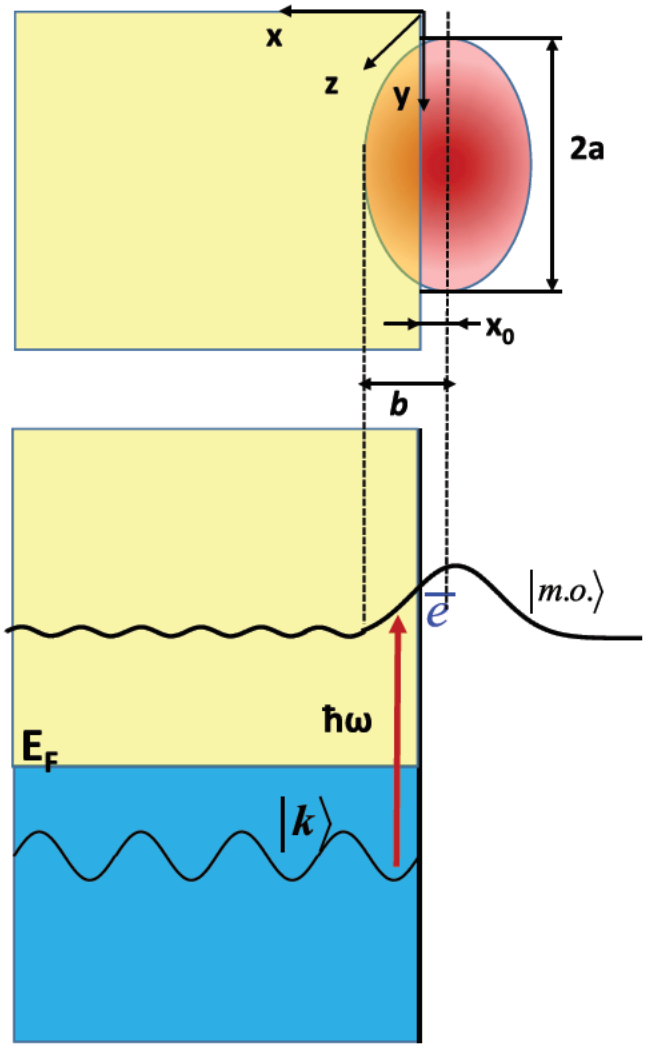


**Figure 2.** Energy levels and wave functions involved in direct absorption.

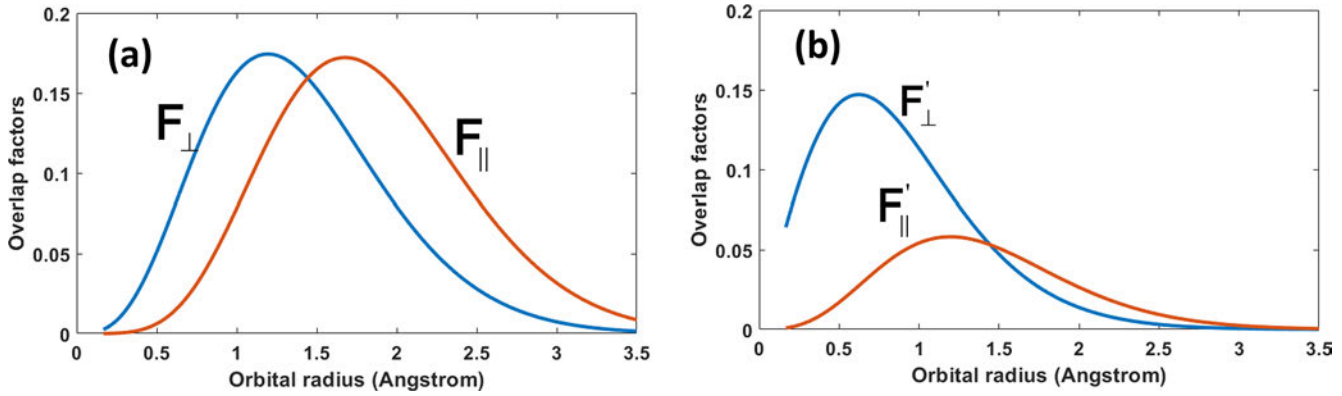


**Figure 3.** Overlap factors $F_\perp$, $F'_\perp$ for normal and $F_\parallel$, $F'_\parallel$ in plane polarizations.

where $\boldsymbol{A} = \boldsymbol{E}/i\omega$ is a vector potential, $p = -i\hbar\nabla$ is momentum, and $m_0$ is a free electron mass. We employ $\boldsymbol{A}\cdot\boldsymbol{p}$ rather than $\boldsymbol{E}\cdot\boldsymbol{r}$ Hamiltonian[50] because the states $|\boldsymbol{k}\rangle$ and $|mo\rangle$ are not orthogonal, hence, using $\boldsymbol{A}\cdot\boldsymbol{p}$ Hamiltonian in place of dipole Hamiltonian assures that the result does not depend on the choice of the origin of coordinates. Let us evaluate the momentum matrix elements for two orthogonal polarizations of the electric field. For the polarization normal to the surface

$$p_\perp = \langle \mathbf{k}|\nabla_x|mo\rangle = \langle k_x|\nabla_x|\Phi_x\rangle\langle k_{y,z}|\Psi_{yz}\rangle = 2a\sqrt{\frac{2\pi C_p}{bL^3}}\frac{k_x b}{(k_x b)^2+1}e^{-k_\parallel^2 a^2/4} \tag{7}$$

where $k_\parallel^2 = k_y^2 + k_z^2$, and for the in plane polarization, where $k_\perp^2 = k_x^2$

$$p_\parallel = \langle \mathbf{k}|\nabla_y|mo\rangle = \langle k_{y,z}|\nabla_{yz}|\Psi_{yz}\rangle\langle k_x|\Phi_x\rangle = 2a\sqrt{\frac{2\pi C_p}{bL^3}}\frac{k_y k_x b^2}{(k_x b)^2+1}e^{-k_\parallel^2 a^2/4} \tag{8}$$

The transition rate to a given molecular orbital can be found using the Fermi Golden rule

$$\begin{aligned} R_{\perp(\parallel)} &= \frac{2\pi}{\hbar}\frac{\hbar^2 e^2}{4m_0^2\omega^2}E_{\perp(\parallel)}^2\sum_{\boldsymbol{k}} p_{\perp(\parallel)}^2\delta\left(E_{mo} - \frac{\hbar^2k^2}{2m_0} - \hbar\omega\right) \\ &\approx \frac{\pi\hbar e^2}{2m_0^2\omega^2}E_{\perp(\parallel)}^2\langle p_{\perp(\parallel)}^2\rangle_{\theta,\varphi}\rho_F L^3 H(\hbar\omega + E_F - E_{mo}) \end{aligned} \tag{9}$$

since integrating over $\boldsymbol{k}$ with a delta function is equivalent to averaging over the direction of $\boldsymbol{k}$ and multiplying by the density of states $\rho(E_{mo} - \hbar\omega) \approx \rho_F = k_F m_0/\pi\hbar^2$, where Heaviside step function $H$ and volume $L^3$ are used. Averaging over the direction means $\langle k_x^2\rangle = \langle k_y^2\rangle = \langle k_z^2\rangle = k_F^2/3$, and therefore, the transition rate for the normal and parallel polarization is

$$R_{\perp(\parallel)} = \frac{4\pi e^2}{m_0\hbar\omega^2}C_p F_{\perp(\parallel)}E_{\perp(\parallel)}^2 H(\hbar\omega + E_F - E_{mo}) \tag{10}$$

where the spatial overlap factors (which are proportional to the square of the transition momentum and thus related to the collective oscillator strength of all the transitions between the continuum states in the metal and a discrete adsorbate state) are

$$\begin{aligned} F_\perp(a,b) &= \frac{\alpha^2}{\beta}\frac{\beta^2/3}{[\beta^2/3+1]^2}e^{-\alpha^2/3} \\ F_\parallel(a,b) &= \frac{\beta^2}{3}F_\perp(a,b) \end{aligned} \tag{11}$$

$\alpha = ak_F$, $\beta = bk_F$, and for gold, $k_F = 1.2$ Å$^{-1}$.

Typically, molecular orbital dimensions $a$ and $b$ are of the same order, so we assume $a = b$ and plot the factors (eq 11) in Figure 3. For realistic values of molecular orbital radii of 1−2 Å, the overlap factors are similar for both polarizations and are on the scale of 0.1. Essentially, the results in Figure 3 indicate that, in order to have a viable direct transition from the extended states in the metal to localized surface states, the spatial Fourier spectrum of the surface state wave function should have a considerable magnitude around the Fermi wavevector. The actual shape of the wave function is not nearly as important as the size of it.

Next, we estimate the CID damping rate if the optical field $E(\boldsymbol{r})$ is confined, then the total rate of energy loss due to absorption into adsorbate states is

$$\begin{aligned} \frac{dU_{CID}}{dt} &= -\hbar\omega N_{ss}\int(R_\perp + R_\parallel)dS \\ &= -\frac{4\pi e^2}{m_0\omega}N_{ss}C_p\int(F_\perp E_\perp^2(\boldsymbol{r}) + F_\parallel E_\parallel^2(\boldsymbol{r}))dS \end{aligned} \tag{12}$$

where $N_{ss}$ is the density of surface states and integration is over the metal surface. Note that $\hbar$ cancels out, which is a good sign as other than overlap factor ("oscillator strength") the result should be classical. At the same time, using the classical Drude formula for the case when the damping rate $\gamma \ll \omega$, we can write the equation for energy loss in the metal particle as

$$\frac{dU}{dt} = -\frac{1}{2}\omega\varepsilon_0\mathrm{Im}[\varepsilon(\omega)]\int_{metal}E^2(\boldsymbol{r})dV = \frac{N_e e^2\gamma}{m_0\omega^2}\int_{metal}E^2(\boldsymbol{r})dV \tag{13}$$

where $N_e$ is the density of electrons, the integral is taken over the field spread inside the metal, and $\gamma$ is the total damping rate that is the sum of the bulk damping rate $\gamma_{bulk}$ and the surface scattering induced damping rate (Landau damping) $\gamma_{LD}$. It is only natural to add CID rate due to direct absorption $\gamma_{CID}^d$ to these processes, that is, set $\gamma = \gamma_{bulk} + \gamma_{LD} + \gamma_{CID}^d + \gamma_{CID}^{sr}$, where $\gamma_{CID}^{sr}$ is a CID contribution due to added surface roughness estimated in SM, so that comparison of eqs 12 and 13 immediately yields a CID rate due to direct absorption

$$\gamma_{CID}^d = 8\pi\omega C_p\frac{N_{ss}}{N_e}\frac{\int(F_\perp E_\perp^2(\boldsymbol{r}) + F_\parallel E_\parallel^2(\boldsymbol{r}))dS}{\int_{metal}E^2(\boldsymbol{r})dV} \tag{14}$$

Note that the last term in eq 14 is an effective surface to volume ratio; hence, the damping rate depends on the ratio of the total number of surface states to the total number of free electron states inside the optical mode volume. To gain further

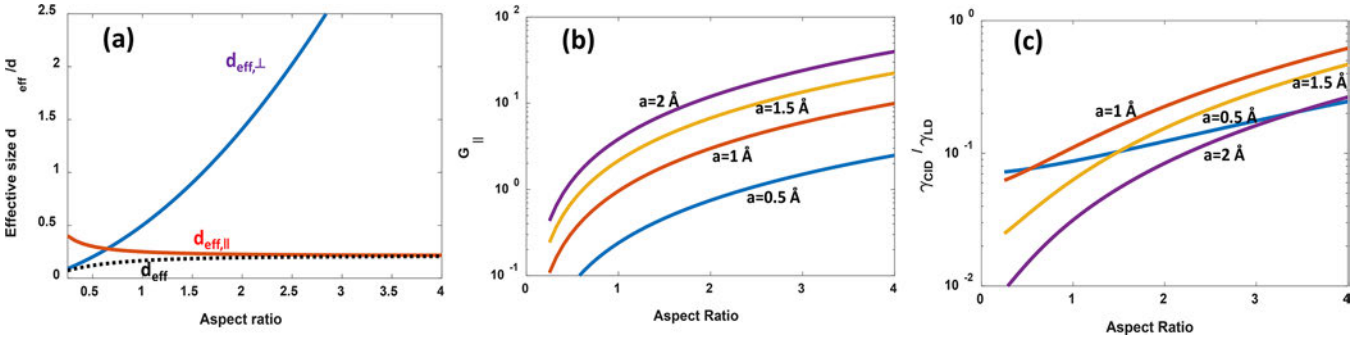


**Figure 4.** (a) Effective size of the ellipsoid for normal and in plane fields. (b) Form factor and (c) ratio of CID to LD rates as a function of aspect ratio of ellipsoidal nanoparticle.

insight, note that the electron density in the metal is $N_e = k_F/3\pi^2$, and one can also introduce the fraction of the surface covered by the adsorbate states $f_{ss} = \pi a^2 N_{ss}$, the one can rewrite eq 14 as

$$\gamma_{CID}^{d} = 24\pi^2 \frac{\omega}{k_F} f_{ss} C_p \left( \frac{F'_\perp}{d_{eff\perp}} + \frac{F'_\parallel}{d_{eff\parallel}} \right) \tag{15}$$

where the modified overlap factors are defined as

$$F'_\perp(a, b) = \frac{1}{\beta} \frac{\beta^2/3}{[\beta^2/3 + 1]^2} e^{-\alpha^2/3}; \quad F'_\parallel(a, b) = \frac{\beta^2}{3} F'_\perp(a, b) \tag{16}$$

and are plotted in Figure 3b, while effective surface to volume ratios for two polarizations are

$$\frac{1}{d_{eff\perp(\parallel)}} = \frac{\int E^2_{\perp(\parallel)}(\boldsymbol{r}) dS}{\int_{metal} E^2(\boldsymbol{r}) dV} \tag{17}$$

Then, what amounts to be "effective sizes" of elliptical nanoparticles with axes $d$ and $md$, $d_{eff,\perp(\parallel)}$ can be plotted relative to diameter $d$ as a function of aspect ratio $m$, as shown in Figure 4a, where also the effective size under the assumption that $F'_\perp \approx F'_\parallel$, $d_{eff} = 1/(d_{eff,\perp}^{-1} + d_{eff,\parallel}^{-1})$ is shown with a dashed line. As one can see, for more or less prolate ellipsoids with $m > 2$, $d_{eff,\parallel} \ll d_{eff,\perp}$, most of CID occurs due to the in plane polarized field, which is precisely the opposite from the LD where it is the normal field that is responsible for hot carrier excitation. Thus, studying samples with oriented prolate nanoparticles, LD and CID can be differentiated by varying the aspect ratio $m$.

## RESULTS

To ascertain the order of magnitude of $\gamma_{CID}$, we first assume a spherical nanoparticle, so that the integration (eq 17) gives $d_{eff,\perp}^{-1} = 6d^{-1}\langle \cos^2\theta \rangle_{\theta,\varphi} = 2d^{-3}$ and $d_{eff,\parallel}^{-1} = 6d^{-1}\langle \sin^2\theta \rangle_{\theta,\varphi} = 4d^{-3}$, leading to $d_{eff,\parallel} = 1/2 d_{eff,\perp} = 0.25d$. Thus, we obtain

$$\gamma_{CID}^{d} \approx 48\pi^2 \frac{\omega}{dk_F} f_{ss} C_p (F'_\perp + 2F'_\parallel) \tag{18}$$

If we assume realistically $F'_\perp \approx F'_\parallel = 0.05$, $C_p = 0.05$, $f_s = 0.1$, and $d = 10$ nm; then, for $\lambda = 700$ nm, we obtain $\gamma_{CID} \sim 8 \times 10^{12}$ s$^{-1}$, which is of course quite small compared to typical damping rates of $\gamma_{bulk} \sim 10^{14}$ s$^{-1}$, as well as[18]

$$\gamma_{LD} = (3/8) v_F / d_{eff,\perp} = 10^{14} \text{ s}^{-1} \tag{19}$$

It is also important to the consider the frequency dependence of the CID effect. As we can see, the CID damping rate is proportional to the frequency of light $\omega$ in contrast to the frequency independent LD. Also, CID damping should drop to zero for $\hbar\omega < E_{mo} - E_F$, which would be a foremost criterion to confirm CID by charge transfer.

To compare with the available experimental data, we consider the results in ref 38, where CID of 15−25 meV has been observed for 66 nm long Au nanorods with 22 nm diameter, 100% covered by thiol adsorbate. We assume that the sulfur atom forms the interface state of radius 1 Å. Approximating the particle shape by an ellipsoid with aspect ratio $m = 3$, increasing $f_{ss}$ to 1 and keeping the same overlap and penetration factors as before, we obtain from eq 15, $\gamma_{CID} \sim 3.0 \times 10^{13}$ s$^{-1}$ or $\hbar\gamma_{CID} \sim 20$ meV, that is, indeed very close to the results of ref 38.

Comparing eq 15 with eq 19, we can obtain the relationship between the rates for CID and LD

$$\frac{\gamma_{CID}^{d}}{\gamma_{LD}} = 64\pi^2 \frac{\omega}{v_F k_F} f_{ss} C_p F'_\perp (1 + G_\parallel) \approx 100 f_{ss} C_p F'_\perp (1 + G_\parallel) \tag{20}$$

where the same $\lambda = 700$ nm has been assumed, and the "form factor" $G_\parallel = (k_F b/3) d_{eff,\parallel}/d_{eff,\perp}$ is plotted as a function of the aspect ratio for different adsorbate molecular orbital radius $b = a$ in Figure 4b. Once again, for $C_p = 0.05$, $f_{ss} = 0.1$, $\gamma_{CID}/\gamma_{LD} \approx 0.5F'_\perp(1 + G_\parallel)$, the relation is shown in Figure 4c. One can see that, as long as the aspect ratio exceeds 2, the CID rate reaches 10% of the LD rate, and if the surface of the nanoparticle is densely covered ($f_{ss}$ approaching 1), the CID may become the dominant damping mechanism. Of course, at 100% coverage, the state in orbitals will couple into 2D extended states on the surface in which the orbitals will play the role of the periodic part of the Bloch states. The extended states will have somewhat reduced responsivity to electric fields parallel to the surface, but $R_\parallel$ will still be distinct from zero, since the Bloch states have spatial Fourier components on the scale of $k_F$ required for the direct transition. In fact, one can consider extended states in energy bands of the semiconductor as the ultimate case of adsorbates with 100% coverage; no wonder then that high efficiencies of direct transfer have been observed on metal−semiconductor interfaces[40,51] for normal fields. But, the adsorbates with dense but not complete coverage might still bare the potential for elongated particles due to additional response to in plane electric fields. One should note that the curve for $a = 0.5$ Å looks different from the curves for larger sizes because, according to Figure 3b, it has large $F'_\perp$ but a very small $F'_\parallel$, which means that the absorption rate does not increase much for the prolate nanoparticles with large aspect ratios.

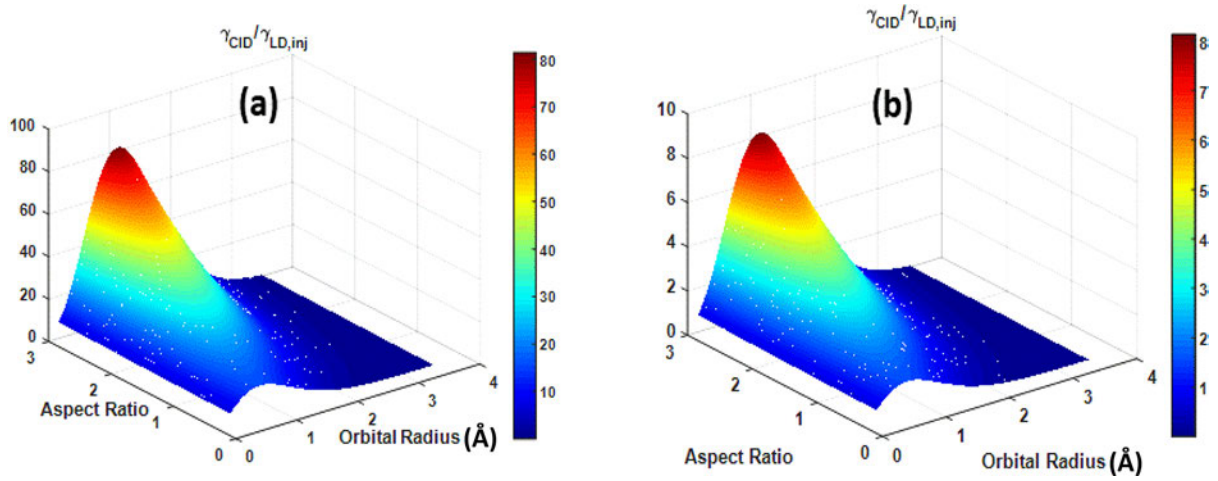


**Figure 5.** Ratio of the direct absorption and carrier injection into the adsorbate states: (a) $C_p/C_{inj} = 1$; (b) $C_p/C_{inj} = 0.1$.

While comparing the different damping rates it is important to appreciate the fact that while all the absorbed carriers directly end up on the adsorbate and can cause chemical reactions, only a small fraction of hot carriers excited by the Landau damping (and even less by other mechanisms[19]) end up on the adsorbate states, let alone participating in chemical reactions. First of all, only the hot carriers excited close to the attached molecule can tunnel onto it. Second, the excited hot carriers must have their energy close to $E_{mo}$. We can therefore introduce a factor $C_{inj}$ to describe the fraction of the carriers that have energies ensuring the transfer into the surface state as well as the efficiency of tunneling (i.e., including probability of reflection back into the metal). Then we can obtain the expression for the injection rate via LD as $\gamma_{inj,LD} = f_{ss}C_{inj}\gamma_{LD}$ and therefore

$$\frac{\gamma^d_{CID}}{\gamma_{inj,LD}} = 64\pi^2\frac{\omega}{v_F k_F}F'_\perp\frac{C_p}{C_{inj}}(1+G_\parallel) \approx 100F'_\perp(a)\frac{C_p}{C_{inj}}[1+G_\parallel(a,m)] \tag{21}$$

The injection factor $C_{inj}$ is relatively easy to calculate for the case of injection from the metal into semiconductor, as in photodetectors, where all the hot electron has to do is to have energy exceeding the potential barrier, and depending on whether the lateral momentum is conserved or not at the boundary, it should have the direction of propagation with a certain solid angle.[19] Depending on the height of the barrier and excess energy this efficiency can be as high as 10−15%. But when it comes to injection into the surface states, the situation is different, as only the carriers with kinetic energies in a relatively narrow range of energies $E_{mo} \pm \Delta E/2$ can transfer to the surface state and $C_{inj} \sim \Delta E/\hbar\omega$. Of course, there exists a possibility that the injection will occur into the higher states of the adsorbate state with the subsequent relaxation to the ground level or to higher states in metal that relax by collision with another electron, but even with that possibility, one cannot expect $C_{inj}$ to exceed 10%. What is also obvious is that the increase in penetration depth $C_p$ and probability of injection $C_{inj}$ occur concurrently, and it is not unreasonable to set their ratio to unity. With that, we can plot the ratio (eq 21) for the aforementioned 700 nm wavelength and for various aspect ratios and adsorbate orbital sizes. We plot for two values of the ratio: $C_p/C_{inj} = 1$ in Figure 5a and $C_p/C_{inj} = 0.1$ in Figure 5b. The second case is probably absolutely the worst case scenario, as it assumes, let us say $C_p = 0.01$, and the latter being highly unrealistic since small $C_p$ implies a very weak hybridization coupling, thus, a narrow resonance for tunneling $\Delta E$, which also brings $C_{inj}$ down. But even for this scenario, there exists a very wide range of parameters within which direct excitation via CID exceeds the excitation via injection of hot carrier, while for a more realistic case of Figure 5a, direct excitation dominates for aspect ratios exceeding 1 and orbital radii $a,b < 2.5$ Å. The situation becomes more dramatic for the elongated geometries, in which such cylindrical nanowires excited by the light polarized along the axis where the normal component of field is very small compared to the in plane one.

## DISCUSSION

So, what is the useful lesson that can be extracted from this relatively straightforward exercise? While the results obtained here are based on a number of assumptions, these assumptions (such as molecular orbital dimension and overlap with metal) look very reasonable to us, and thus, we believe that our results provide a right order of magnitude estimate of the direct absorption of carriers (electrons or holes) from the extended states in the metal to the molecules attached to the surface. What seems to be beyond the doubt to us is that since 100% of the carriers excited by direct absorption may contribute to chemical reaction, the rate of this process is easily comparable or exceeds the rate of the indirect injection of photoexcited carriers, where most of the carriers end up on the Fermi level within tens of femtoseconds. Our results are corresponding quantitatively to the experimental observations of CID from thiol adsorbates,[38,41,46] especially the strong effect on elongated particles.

And what is the actual charge transfer efficiency? Though several attempts exist to characterize direct charge transfer,[30,33,40,42,51] the quantum efficiency of this process had only been determined for the cases of semiconductors only.[29,40,51] From our theory, we can estimate the efficiency of charge transfer by comparison to all possible excitations:

$$\eta_{ct} = \frac{\gamma^d_{CID} + \gamma_{inj,LD} + C_{inj}\gamma^{sr}_{CID}}{\gamma^d_{CID} + \gamma^{sr}_{CID} + \gamma_{LD} + \gamma_{bulk}} \tag{22}$$

Now, for the elongated nanoparticles $\gamma_{inj,LD} \ll \gamma^d_{CID}$ in accordance with eq 21 and following SM $\gamma^{sr}_{CID} \ll \gamma^d_{CID}$. The latter is a consequence of direct absorption being a first order

excitation process, and roughness assisted excitation being a second order process with virtual states involved. Expressing $\gamma_{bulk}$ via $\gamma_{LD}$ from eq 19, we obtain using eq 20

$$\eta_{ct} \approx \frac{100 f_{ss} C_p F'_{\perp}(1 + G_{\parallel})}{100 f_{ss} C_p F'_{\perp}(1 + G_{\parallel}) + 1 + 0.2 d_{eff,\perp}} \quad (23)$$

where $d_{eff,\perp}$ is in nm. For $d_{eff,\perp} < 5$ nm, the bulk damping becomes insignificant, and according to Figure 4c for such small spherical particles with 10% surface coverage by adsorbate charge transfer efficiency is less than 10%, but for the elongated particles with aspect ratio of 3, it can be increased to 15−18%. With 100% coverage, though 50% can be within reach. The use of transferred charges for chemical reactions being the final goal for plasmonic catalysis, it should also be mentioned that far from all directly excited carriers later participate in chemical reactions as there is a strong possibility for the charge to return into the metal before the reaction takes place. Recently, the photocurrent with quantum efficiency of only 0.1% was measured by the direct charge transfer from nanoporous gold into −OH adsorbates.[30] It should be noted that the transferred carrier may also cause vibrational heating in the adsorbate, which by itself can accelerate the chemical reaction even if the carrier eventually returns to the metal,[45] but that process would also benefit if the electrons stay in the adsorbate for the appreciable period of time. Unfortunately, the return mechanism also depends on the overlap between molecular orbital and metal electron states, that is, the coupling works bidirectionally. The unavoidable fact is that the density of states available for carriers in the metal is much larger than density of states in adsorbate, so the carriers would always tend to leak back into the metal. That is why the carrier transfer into the semiconductor, with its relatively large density of states and 100% coverage, is more promising for achieving higher efficiencies. Also, in semiconductors, the existence of the Schottky barrier allows to keep the charges in the semi conductor by fast thermalization to the lower band edge. Accordingly, to increase the photocatalytic efficiency in adsorbates, mechanisms should be identified that quickly transfer the electron to a lower, metastable state with reduced coupling to the metal states. Also, for isolated, not electrically connected, particles both oxidation and reduction reactions should run to balance the charge, which additionally reduces efficiency. More promising in this respect is the application of conductive photoelectrodes, where only one partial reaction has to run on one electrode.[20,30,52,53]

The beneficial role of plasmons as pertained to the acceleration of chemical reactions is 2 fold. First, the presence of metal nanoparticles provides local field enhancement, so more light gets absorbed by adsorbates, and second, since the direct transitions originate at the continuum of electron states below the Fermi level, even though the energy eigenvalues $E_{mo}$ of the hybrid state are discrete, the direct process is still broadband, that is, can be driven by the white light coming from the sun. What is particularly important is that even a relatively long wavelength radiation can still be used as long as $\hbar\omega > E_{mo} - E_F$. Thus, the metal nanoparticles enable efficient electron transfer even below the HOMO−LUMO resonance, that is, when no photochemical reaction can take place on isolated molecules. In the calculation presented here we have considered free electrons inside metal that represent s band electrons. At higher photon energies, also, d band electrons can be excited, which we have not considered and which require a different approach. Of course, everything said about the excitation of an electron from the conduction band into the adsorbate state, ultimately causing a reductive chemical reaction, can be equally well applied to the excitation from the adsorbate state into the empty state in the conduction band, creating a hole in the adsorbate state, available for a further oxidative chemical reaction. Due to the availability of empty states in the conduction band above $E_F$, also, this process is broadband.

Next comes the question of how can one enhance the efficiency of the directly plasmon induced chemical reactions? On the basis of our analysis, a set of recommendations can be made. (1) Use smaller nanoparticles with larger surface to volume ratio so that surface absorption dominates the bulk absorption. (2) The particles should be prolate with aspect ratios exceeding 2 or 3 to enhance the direct absorption relative to LD. (3) Most obviously, the coverage of the nanoparticle by the adsorbate $f_{ss}$ must be optimized, perhaps taking into account shifts of the hybrid state energies and coupling. (4) The transferred charge should stay in the adsorbate until it is consumed in the chemical reaction. Thus, the charge should lead to chemical transformation of the adsorbate itself or lead to detachment of the adsorbate with the charge which would make it necessary to later redeposit the adsorbates on the metal surface in a cycle. Such concepts and questions are beyond the scope of this paper.

## CONCLUSIONS

It is our conclusion then that direct absorption from metal into adsorbate states must never be overlooked in plasmonic assisted chemical reaction studies. This conclusion may help in explaining a number of the experimental results, where the observed rates of reaction were too high to be explained solely by the hot carrier injection. This work also should serve as a motivation for the experimental community to find new and better ways of distinguishing between direct absorption and injection and then to optimize the nanoparticle geometries and nature of adsorbate states to further enhance the reaction rates and efficiencies.

## AUTHOR INFORMATION


### Corresponding Author

Jacob B Khurgin − *Department of ECE, Johns Hopkins University, Baltimore, Maryland 21218, United States;* orcid.org/0000 0003 0725 8736; Email: jakek@jhu.edu

### Authors

Alexander Petrov − *Institute of Optical and Electronic Materials, Hamburg University of Technology, Hamburg 21073, Germany; Institute of Materials Research, Helmholtz Zentrum Geesthacht Centre for Materials and Coastal Research, Geesthacht 21502, Germany; Research Institute for Optical Materials Science, ITMO University, Saint Petersburg 199034, Russia*

Manfred Eich − *Institute of Optical and Electronic Materials, Hamburg University of Technology, Hamburg 21073, Germany; Institute of Materials Research, Helmholtz Zentrum Geesthacht Centre for Materials and Coastal Research, Geesthacht 21502, Germany*
Alexander V. Uskov − *P. N. Lebedev Physical Institute of Russian Academy of Sciences, Moscow 119991, Russia*

### Notes

The authors declare no competing financial interest.

## ■ ACKNOWLEDGMENTS

J.K. acknowledges the Air Force Office of Scientific Research (FA9550 16 10362). A.P. and M.E. gratefully acknowledge financial support from the Deutsche Forschungsgemeinschaft DFG, German Research Foundation) − Projektnummer 192346071 − SFB 986. A.P. and A.U. are thankful to the Russian Science Foundation (Grant 20 19 00559) for support. J.K. would also like to express his gratitude to Prof. P. Noir and Dr. S. Artois for illuminating discussions.

## ■ REFERENCES

(1) Stockman, M. I. Nanoplasmonics: past, present, and glimpse into future. *Opt. Express* **2011**, *19* (22), 22029−22106.
(2) Maier, S. A. *Plasmonics: Fundamentals and Applications*; Springer: New York, 2007; p xxiv.
(3) Khurgin, J. B. How to deal with the loss in plasmonics and metamaterials. *Nat. Nanotechnol.* **2015**, *10* (1), 2−6.
(4) Stewart, M. E.; Anderton, C. R.; Thompson, L. B.; Maria, J.; Gray, S. K.; Rogers, J. A.; Nuzzo, R. G. Nanostructured plasmonic sensors. *Chem. Rev.* **2008**, *108* (2), 494−521.
(5) Zhang, S. P.; Bao, K.; Halas, N. J.; Xu, H. X.; Nordlander, P. Substrate Induced Fano Resonances of a Plasmonic: Nanocube: A Route to Increased Sensitivity Localized Surface Plasmon Resonance Sensors Revealed. *Nano Lett.* **2011**, *11* (4), 1657−1663.
(6) Bozhevolnyi, S. I.; Khurgin, J. B. The case for quantum plasmonics. *Nat. Photonics* **2017**, *11* (7), 398−400.
(7) Aizpurua, J.; Baumberg, J.; Boltasseva, A.; Christopher, P.; Cortes, E.; Cronin, S. B.; Dadhich, B. K.; de Nijs, B.; Deshpande, P.; Fernandez, Y. D.; Fabris, L.; Gawinkowski, S.; Govorov, A.; Halas, N.; Huang, J. Y.; Jankiewicz, B.; Kamarudheen, R.; Khurgin, J.; Lee, T. K.; Mahin, J.; Marini, A.; Maurer, R. J.; Mueller, N. S.; Park, J. Y.; Rahaman, M.; Schlucker, S.; Schultz, Z.; Sivan, Y.; Tagliabue, G.; Thangamuthu, M.; Xu, H. X.; Zayats, A. New materials for hot electron generation: general discussion. *Faraday Discuss.* **2019**, *214*, 365−386.
(8) Goykhman, I.; Desiatov, B.; Khurgin, J.; Shappir, J.; Levy, U. Locally Oxidized Silicon Surface Plasmon Schottky Detector for Telecom Regime. *Nano Lett.* **2011**, *11* (6), 2219−2224.
(9) Lal, S.; Clare, S. E.; Halas, N. J. Nanoshell Enabled Photo thermal Cancer Therapy: Impending Clinical Impact. *Acc. Chem. Res.* **2008**, *41* (12), 1842−1851.
(10) Zhou, L. A.; Swearer, D. F.; Zhang, C.; Robatjazi, H.; Zhao, H. Q.; Henderson, L.; Dong, L. L.; Christopher, P.; Carter, E. A.; Nordlander, P.; Halas, N. J. Quantifying hot carrier and thermal contributions in plasmonic photocatalysis. *Science* **2018**, *362* (6410), 69.
(11) Mukherjee, S.; Libisch, F.; Large, N.; Neumann, O.; Brown, L. V.; Cheng, J.; Lassiter, J. B.; Carter, E. A.; Nordlander, P.; Halas, N. J. Hot Electrons Do the Impossible: Plasmon Induced Dissociation of H 2 on Au. *Nano Lett.* **2013**, *13* (1), 240−247.
(12) Aizpurua, J.; Baumberg, J.; Caps, V.; Cortes, E.; de Nijs, B.; Fernandez, Y. D.; Fabris, L.; Freakley, S.; Gawinkowski, S.; Glass, D.; Huang, J. Y.; Jankiewicz, B.; Khurgin, J.; Kumar, P. V.; Maurer, R. J.; McBreen, P.; Mueller, N. S.; Park, J. Y.; Quiroz, J.; Rejman, S.; Gomez, R. M. R.; Salmon Gamboa, J.; Schlucker, S.; Schultz, Z.; Shukla, A.; Sivan, Y.; Thangamuthu, M.; Torrente Murciano, L.; Xiao, X. F.; Xu, H. X.; Zhan, C. Applications in catalysis, photochemistry, and photodetection: general discussion. *Faraday Discuss.* **2019**, *214*, 479−499.
(13) Zhang, Y. C.; He, S.; Guo, W. X.; Hu, Y.; Huang, J. W.; Mulcahy, J. R.; Wei, W. D. Surface Plasmon Driven Hot Electron Photochemistry. *Chem. Rev.* **2018**, *118* (6), 2927−2954.
(14) Xu, X. H.; Dutta, A.; Khurgin, J.; Wei, A. L.; Shalaev, V. M.; Boltasseva, A. Plasmonic Photosensitizers: TiN@$TiO_2$ Core Shell Nanoparticles as Plasmon Enhanced Photosensitizers: The Role of Hot Electron Injection. *Laser Photonics Rev.* **2020**, *14* (5), 2070031.
(15) Ozawa, K.; Yamamoto, S.; Yukawa, R.; Liu, R. Y.; Terashima, N.; Natsui, Y.; Kato, H.; Mase, K.; Matsuda, I. Correlation between Photocatalytic Activity and Carrier Lifetime: Acetic Acid on Single Crystal Surfaces of Anatase and Rutile TiO2. *J. Phys. Chem. C* **2018**, *122* (17), 9562−9569.
(16) Tagliabue, G.; DuChene, J. S.; Abdellah, M.; Habib, A.; Gosztola, D. J.; Hattori, Y.; Cheng, W. H.; Zheng, K.; Canton, S. E.; Sundararaman, R.; Sá, J.; Atwater, H. A. Ultrafast hot hole injection modifies hot electron dynamics in Au/p GaN heterostructures. *Nat. Mater.* **2020**, *19* (12), 1312−1318.
(17) Grajower, M.; Levy, U.; Khurgin, J. B. The Role of Surface Roughness in Plasmonic Assisted Internal Photoemission Schottky Photodetectors. *ACS Photonics* **2018**, *5* (10), 4030−4036.
(18) Khurgin, J. B. Hot carriers generated by plasmons: where are they generated and where do they go from there? *Faraday Discuss.* **2019**, *214*, 35−58.
(19) Khurgin, J. B. Fundamental limits of hot carrier injection from metal in nanoplasmonics. *Nanophotonics* **2020**, *9* (2), 453−471.
(20) Reddy, H.; Wang, K.; Kudyshev, Z.; Zhu, L.; Yan, S.; Vezzoli, A.; Higgins, S. J.; Gavini, V.; Boltasseva, A.; Reddy, P.; Shalaev, V. M.; Meyhofer, E. Determining plasmonic hot carrier energy distributions via single molecule transport measurements. *Science* **2020**, *369* (6502), 423−426.
(21) Dubi, Y.; Sivan, Y. "Hot" electrons in metallic nanostructures non thermal carriers or heating? *Light: Sci. Appl.* **2019**, *8*, na.
(22) Sivan, Y.; Baraban, J.; Un, I. W.; Dubi, Y. Comment on "Quantifying hot carrier and thermal contributions in plasmonic photocatalysis". *Science* **2019**, *364*, 6439.
(23) Sivan, Y.; Un, I. W.; Dubi, Y. Assistance of metal nanoparticles in photocatalysis nothing more than a classical heat source. *Faraday Discuss.* **2019**, *214*, 215−233.
(24) Sivan, Y.; Dubi, Y. Recent developments in plasmon assisted photocatalysis A personal Perspective. *Appl. Phys. Lett.* **2020**, *117* (13), 130501.
(25) Khurgin, J. B.; Levy, U. Generating Hot Carriers in Plasmonic Nanoparticles: When Quantization Does Matter? *ACS Photonics* **2020**, *7* (3), 547−553.
(26) Uskov, A. V.; Protsenko, I. E.; Mortensen, N. A.; O'Reilly, E. P. Broadening of Plasmonic Resonance Due to Electron Collisions with Nanoparticle Boundary: A Quantum Mechanical Consideration. *Plasmonics* **2014**, *9* (1), 185−192.
(27) Uskov, A. V.; Protsenko, I. E.; Ikhsanov, R. S.; Babicheva, V. E.; Zhukovsky, S. V.; Lavrinenko, A. V.; O'Reilly, E. P.; Xu, H. X. Internal photoemission from plasmonic nanoparticles: comparison between surface and volume photoelectric effects. *Nanoscale* **2014**, *6* (9), 4716−4727.
(28) Ratchford, D. C.; Dunkelberger, A. D.; Vurgaftman, I.; Owrutsky, J. C.; Pehrsson, P. E. Quantification of Efficient Plasmonic Hot Electron Injection in Gold Nanoparticle TiO2 Films. *Nano Lett.* **2017**, *17* (10), 6047−6055.
(29) Ratchford, D. C. Plasmon Induced Charge Transfer: Challenges and Outlook. *ACS Nano* **2019**, *13* (12), 13610−13614.
(30) Graf, M.; Vonbun Feldbauer, G. B.; Koper, M. T. M. Direct and Broadband Plasmonic Charge Transfer to Enhance Water Oxidation on a Gold Electrode. *ACS Nano* **2021**, *15*, 3188−3200.

(31) Hovel, H.; Fritz, S.; Hilger, A.; Kreibig, U.; Vollmer, M. Width of Cluster Plasmon Resonances Bulk Dielectric Functions and Chemical Interface Damping. *Phys. Rev. B: Condens. Matter Mater. Phys.* **1993**, *48* (24), 18178−18188.
(32) Tan, S.; Dai, Y.; Zhang, S.; Liu, L.; Zhao, J.; Petek, H. Coherent Electron Transfer at the $\mathrm{Ag}/\mathrm{Graphite}$ Heterojunction Interface. *Phys. Rev. Lett.* **2018**, *120* (12), 126801.
(33) Boerigter, C.; Campana, R.; Morabito, M.; Linic, S. Evidence and Implications of Direct Charge Excitation as the Dominant Mechanism in Plasmon Mediated Photocatalysis. *Nat. Commun.* **2016**, *7*, 10545.
(34) Kreibig, U. Interface induced dephasing of Mie plasmon polaritons. *Appl. Phys. B: Lasers Opt.* **2008**, *93* (1), 79−89.
(35) Marom, H.; Eizenberg, M. The effect of surface roughness on the resistivity increase in nanometric dimensions. *J. Appl. Phys.* **2006**, *99* (12), 123705.
(36) Lin, K. C.; Tobin, R. G.; Dumas, P.; Hirschmugl, C. J.; Williams, G. P. Adsorbate induced changes in the infrared reflectance and resistivity of metals. *Phys. Rev. B: Condens. Matter Mater. Phys.* **1993**, *48* (4), 2791−2794.
(37) Hakamada, M.; Kato, N.; Mabuchi, M. Electrical resistivity of nanoporous gold modified with thiol self assembled monolayers. *Appl. Surf. Sci.* **2016**, *387*, 1088−1092.
(38) Foerster, B.; Spata, V. A.; Carter, E. A.; Sönnichsen, C.; Link, S. Plasmon damping depends on the chemical nature of the nanoparticle interface. *Science Advances* **2019**, *5* (3), eaav0704.
(39) Persson, B. N. J. Polarizability of Small Spherical Metal Particles: Influence of the Matrix Environment. *Surf. Sci.* **1993**, *281*, 153.
(40) Wu, K.; Chen, J.; McBride, J. R.; Lian, T. Efficient hot electron transfer by a plasmon induced interfacial charge transfer transition. *Science* **2015**, *349* (6248), 632−635.
(41) Foerster, B.; Joplin, A.; Kaefer, K.; Celiksoy, S.; Link, S.; Sönnichsen, C. Chemical Interface Damping Depends on Electrons Reaching the Surface. *ACS Nano* **2017**, *11*, 2886.
(42) Boerigter, C.; Aslam, U.; Linic, S. Mechanism of Charge Transfer from Plasmonic Nanostructures to Chemically Attached Materials. *ACS Nano* **2016**, *10* (6), 6108−6115.
(43) Kale, M. J.; Avanesian, T.; Christopher, P. Direct Photocatalysis by Plasmonic Nanostructures. *ACS Catal.* **2014**, *4* (1), 116−128.
(44) Foerster, B.; Hartelt, M.; Collins, S. S. E.; Aeschlimann, M.; Link, S.; Sönnichsen, C. Interfacial States Cause Equal Decay of Plasmons and Hot Electrons at Gold−Metal Oxide Interfaces. *Nano Lett.* **2020**, *20* (5), 3338−3343.
(45) Boerigter, C.; Campana, R.; Morabito, M.; Linic, S. Evidence and implications of direct charge excitation as the dominant mechanism in plasmon mediated photocatalysis. *Nat. Commun.* **2016**, *7* (1), 10545.
(46) Zijlstra, P.; Paulo, P. M. R.; Yu, K.; Xu, Q. H.; Orrit, M. Chemical Interface Damping in Single Gold Nanorods and Its Near Elimination by Tip Specific Functionalization. *Angew. Chem., Int. Ed.* **2012**, *51* (33), 8352−8355.
(47) Khurgin, J. B. Ultimate limit of field confinement by surface plasmon polaritons. *Faraday Discuss.* **2015**, *178*, 109−122.
(48) Kotur, M.; Guénot, D.; Jiménez Galán, Á.; Kroon, D.; Larsen, E. W.; Louisy, M.; Bengtsson, S.; Miranda, M.; Mauritsson, J.; Arnold, C. L.; Canton, S. E.; Gisselbrecht, M.; Carette, T.; Dahlström, J. M.; Lindroth, E.; Maquet, A.; Argenti, L.; Martín, F.; L'Huillier, A. Spectral phase measurement of a Fano resonance using tunable attosecond pulses. *Nat. Commun.* **2016**, *7* (1), 10566.
(49) Fano, U. Effects of Configuration Interaction on Intensities and Phase Shifts. *Phys. Rev.* **1961**, *124* (6), 1866−1878.
(50) Cohen Tannoudji, C.; Dupont Roc, J.; Grynberg, G. *Atom−photon interactions: basic processes and applications*; Wiley: New York, 1992; p xxii.
(51) Kumar, P. V.; Rossi, T. P.; Marti Dafcik, D.; Reichmuth, D.; Kuisma, M.; Erhart, P.; Puska, M. J.; Norris, D. J. Plasmon Induced Direct Hot Carrier Transfer at Metal−Acceptor Interfaces. *ACS Nano* **2019**, *13* (3), 3188−3195.
(52) Graf, M.; Jalas, D.; Weissmüller, J.; Petrov, A. Y.; Eich, M. Surface to Volume Ratio Drives Photoelelectron Injection from Nanoscale Gold into Electrolyte. *ACS Catal.* **2019**, *9* (4), 3366−3374.
(53) Watanabe, T.; Gerischer, H. Photoelectrochemical studies on gold electrodes with surface oxide layers: Part II. Discrimination between the surface photoprocess and photohole emission. *J. Electroanal. Chem. Interfacial Electrochem.* **1981**, *122*, 73−91.